Journal of Photochemistry & Photobiology, A: Chemistry 408 (2021) 113091

Contents lists available at ScienceDirect

Journal of Photochemistry & Photobiology, A: Chemistry

journal homepage: www.elsevier.com/locate/jphotochem

Investigating the influence of silver state on electronic properties of Ag/Ag_2O/TiO_2 heterojunctions prepared by photodeposition

A.A. Vodyankin [a], Yu.A. Belik [a], V.I. Zaikovskii [b], O.V. Vodyankina [a,*]

[a] National Research Tomsk State University, Tomsk, Russia
[b] Institute of Catalysis Siberian Branch of Russian Academy of Science, Novosibirsk, Russia

ARTICLE INFO

Keywords:
Silver nanoparticles
Titania
Photoreduction
Reaction mechanism
Sensitization
Photocatalysis
Rhodamine B

ABSTRACT

Two series of Ag-TiO_2 photocatalysts were prepared with the use of photodeposition method with variation of the irradiation time and precursor concentration. The obtained photocatalysts were studied by XRD, Raman spectroscopy, HR TEM, UV–vis spectroscopy, and low-temperature N_2 adsorption/desorption method. It has been consequently found that the optical properties of the resulting catalysts differ significantly: the positions of surface plasmon resonance peaks red-shifted with the increase in precursor concentration. At the same time, optical absorption of the samples increases with both precursor concentration and irradiation time. Photocatalytic activity for the obtained catalysts was evaluated in decolorization of Rhodamine B with the use of Xe arc lamp (250 W) with and without $\lambda > 420$ nm light filter. Radical trap experiments have shown that the amount of both superoxide anions and hydroxyl radicals increased in full spectrum of the lamp, with the latter being absent in the reaction mixture during visible light photocatalysis. Comparison of different Ag-TiO_2 catalysts has also been made, with 1-Ag-90 min sample being the most active in full spectrum, and 3-Ag-90 min demonstrating the highest conversion in visible light attributed to the increased generation of superoxide species on the surface of Ag clusters. Controversially, 1-Ag-45 min sample showed the lowest activity in full spectrum being surpassed even by unmodified TiO_2, but reached the highest rate constant value in visible light. This effect can be related to advanced electronic interaction between Ag plasmonic nanoparticles and titania support in the presence of sensitizer compound, and the formation of Ag/Ag_2O composite system on the surface of titania. Influence of the state of silver on photocatalytic activity and mechanism details is discussed with special attention to irradiation wavelengths.

1. Introduction

In the course of time, a selection of titania-based studies has been featuring photocatalytic silver and its effect on photocatalytic activity in oxidation of organic compounds [1]. Some of the most recent works feature the development of Ag/Ag_2O/TiO_2 heterojunctions [2–4]. Such catalytic systems are known for their notable ability to participate in visible light-driven reactions of photodegradation and water oxidation, which is supported by increased generation of oxidant species due to the realization of Z-scheme charge transfer mechanism. A common important issue of Ag^+ ions being reduced during the photocatalytic experiment is also negated in such type of heterojunctions [5,6], which makes Ag/Ag_2O/TiO_2 promising silver-based photocatalytic systems for decomposing organic pollutants. Amongst preparation methods, chemical reduction [7], liquid impregnation [8,9], sol-gel [10], and photoreduction [11] are some of the most commonly used. While many methods are proven to yield significant improvement of photocatalytic activity, photoreduction method stands out because of better involvement of the support matrix in electron transfer during the process of photodeposition [12] and relative simplicity and predictability of the reduction process where Ag^+ ions require less additional agents or control measures to be reduced to metallic silver if required [13]. Such catalysts are considered an appealing solution for reactions of dye photodegradation, such as Rhodamine B [14–16], methyl orange [17,18], methylene blue [11], and a selection of others [19,20].

The important factors of Ag positive influence in photooxidation reactions were cited as narrowing of the band gap [21], increased generation of superoxide radical and hydroxyl radical species [22,23], increased charge carrier separation [24], increased adsorption capacity [22], and enhanced wettability [25]. At the same time, a general trend

* Corresponding author.
E-mail address: vodyankina_o@mail.ru (O.V. Vodyankina).

https://doi.org/10.1016/j.jphotochem.2020.113091
Received 29 August 2020; Received in revised form 6 November 2020; Accepted 7 December 2020
Available online 8 December 2020

for Ag particles is observed, where, after a certain point, increased metallic properties of the loaded silver aggregate lead to an activity reduction due to silver sites becoming responsible for hole recombination and hindering access of organic species to the titania surface [26]. However, there is still a lot of ambiguity in how the state of Ag on the surface of TiO_2 does affect the photodegradation mechanism, and how electronic interactions between Ag nanoparticles and TiO_2 support might contribute to such differences. Several studies also point out on a detrimental effect of silver presence in TiO_2-based photocatalysts, sometimes without further comments [22].

In this work, two series of $Ag/Ag_2O/TiO_2$ photocatalysts are prepared via photoreduction method using 250 W Xe arc lamp, where irradiation time and Ag precursor concentration were varied in respective synthesis procedures, while commercial TiO_2 P25 photocatalyst was used as a support in both cases. To investigate the effect of silver on photocatalytic activity and electronic properties of TiO_2, Rhodamine B dye was used capable of sensitizing TiO_2 with the use of visible light energy [27]. Generation of active species for pristine TiO_2 sample (Degussa P25) and silver-loaded samples was investigated with the use of $^{\bullet}O_2^-$ and $^{\bullet}OH$ radical traps. In all experiments, both visible and combined UV + Vis spectra of a 250 W Xe arc lamp were used.

2. Experimental

The following compounds were used in synthesis procedure and photocatalytic tests: titanium dioxide (Merck, Germany), silver nitrate (Regionchemshab, Russia), Rhodamine B (Vekton, Russia), isopropyl alcohol (EKOS-1, Russia), benzoquinone (Vekton, Russia). All the chemicals applied were of analytical grade and used without further purifications.

$Ag/Ag_2/TiO_2$ photocatalysts were prepared via typical photodeposition method [28]. Commercial TiO_2 P25 was used as a substrate. During the preparation of samples, two key factors were varied: (i) concentration of Ag precursor, from 1.16 to 6.95 mM; (ii) irradiation time, from 45 min to 270 min. 40 mL of $AgNO_3$ aqueous solution of desired concentration and 1 g of commercial TiO_2 P25 (as-received) were placed in 50 mL glass beaker and irradiated by 250 W Xe arc lamp during a chosen time in air atmosphere under constant vigorous stirring. After the irradiation, the samples were rinsed with distilled water, filtered and dried in a desiccator in dark for 24 h. No thermal treatment was applied.

In the first series of the samples, the irradiation times were varied from 45 min to 270 min, while the initial concentration of $AgNO_3$ was fixed at 2.32 mmol/L. The obtained photocatalysts were subsequently designated as 1-Ag-45 min, 1-Ag-90 min, and 1-Ag-270 min, where "1″ stood for the proportion coefficient for Ag^+ concentration.

The second sample series were prepared with the fixed irradiation time of 90 min. At the same time, initial $AgNO_3$ concentrations were varied within the range of 1−5 mmol/L. The resulting samples were titled as 0.5-Ag-90 min, 1-Ag-90 min, and 2-Ag-90 min. The sample names represent the preparation details – the first number stands for a proportion coefficient for Ag^+ concentration, while the last number is designated for the irradiation time.

Optical properties of the samples were studied with the use of Evolution-600 (Thermo Scientific, USA) spectrometer in diffuse reflectance mode. Stock MgO standard was used as reference. The samples were studied without dilution. Optical bandgaps were calculated via conventional Tauc plot method for indirect transitions.

The textural features of the prepared samples were analyzed by low-temperature N_2 adsorption/desorption method using the TriStar II 3020 analyzer (Micromeritics, United States) and calculated using the BJH method to determine the micropore size distributions.

The elemental composition of the samples was analyzed using the X-ray fluorescence (XRF) wavelength-dispersive sequential spectrometer XRF-1800 (Shimadzu, Japan). X-ray diffraction (XRD) patterns were recorded using the XRD-6000 diffractometer (Shimadzu, Japan) with a monochromatized Cu Kα radiation (λ = 1.5418 Å) in the range of angles of 20–70 (2θ) with a scanning rate of 2°/min. Raman spectroscopy measurements were performed using of InVia microscope (Renishaw, UK) with laser excitation at a wavelength of 532 nm in the range of 100–1000 cm^{-1} at a power less than 1 mW.

Transmission electron microscopy (TEM) data were obtained using the JEM-2200 FS (JEOL, Japan) microscope with a resolution of 0.1 nm at an accelerating voltage of 200 kV. High-angle annular dark-field scanning transmission electron microscopy (HAADF-STEM) was used to analyze the features of distribution of silver nanoparticles on titania surface. The crystal lattice parameters were calculated by Fourier transform using the DigMicrograph (GATAN) software.

The electrokinetic properties of the suspensions were studied with an Omni S/N analyzer (Brookhaven, USA) equipped with a BI-ZTU autotitrator. To measure the particle electrophoretic mobility and calculate the zeta potential, the phase analysis light scattering technique was used. The pH of the zero charge point for the colloidal solutions were measured by titration using diluted (0.001 and 0.1 mol/L) solutions of KOH or HNO_3. To measure the dynamics of zeta potential in water suspensions of TiO_2 and Ag/TiO_2 samples, a concentration of 30–50 mg/L was used, being prepared with distilled water.

All discussed samples as well as unmodified TiO_2 were tested in a 40 mL batch reactor with a quartz window. The amount of catalyst was 50 mg with Rhodamine B (RhB) chosen as substrate. The starting concentration of RhB was $2 \cdot 10^{-5}$ M. Suspension with the catalyst and substrate was kept in dark for 1 h and irradiated for 4 h under constant stirring, with an aliquot of 4 mL centrifuged and analyzed every hour via SOLAR PB 2201 spectrophotometer (Solar, Belarus) in optical density mode. A $\lambda > 420$ nm cut-off filter was employed in experiments involving visible light. 250 W Xe arc lamp was used in all photocatalytic experiments. During radical trapping experiments, benzoquinone and isopropyl alcohol were used as scavengers for superoxide radicals and hydroxyl radicals, respectively. The amounts of introduced scavengers were chosen according to literature data in a similar experiment with regards to catalyst mass and solution volume: 0.001 M for benzoquinone and 0.02 M for isopropyl alcohol [29]. To ensure the correctness of chosen isopropyl alcohol concentration, an additional series of experiments with Rhodamine B photodecolorization by pristine TiO_2 P25 was conducted.

3. Results and discussion

Table 1 lists the synthesized samples and their preparation details. The C_{Ag+} column contains data on initial concentration of $AgNO_3$ during preparation of the Ag/TiO_2 systems; t_{ir} stands for irradiation time in the synthesis performed. The weight fractions of silver in the prepared samples detected via X-ray fluorescence analysis are listed in the ω_{Ag} column. Optical properties of the samples are featured in λ_{SPR} and E_g columns providing locations of surface plasmon resonance peaks and optical bandgap values, respectively.

According to the presented data, irradiation time and initial Ag^+ concentration have an impact on the silver content in the obtained samples: the weight percentage of Ag is increased with both factors. However, only 0.5-Ag-90 min sample corresponds to theoretical

Table 1
Titania-based samples featured in the study.

Sample	C_{Ag+}, mM	t_{ir}, min	ω_{Ag}*, % wt.	λ_{SPR}, nm	E_g, eV
1-Ag-45 min	**2.32**	45	0.55	512	2.80 ± 0.02
1-Ag-90 min	**2.32**	90	0.74	518	2.88 ± 0.02
1-Ag-270 min	**2.32**	270	0.68	518	2.75 ± 0.02
0.5-Ag-90 min	1.16	**90**	0.51	488	2.91 ± 0.02
1-Ag-90 min	2.32	**90**	0.74	518	2.88 ± 0.02
2-Ag-90 min	4.64	**90**	0.70	532	2.83 ± 0.02
TiO_2 P25	–	–	0	–	3.10 ± 0.02

* according to XRF data.

expectations, having ~0.51 % wt. according to the XRF results. In case of other samples, the Ag content does not exceed 0.74 % wt. for double $AgNO_3$ concentration (1-Ag-90 min), and all other samples including 2-Ag-90 min show lesser amounts. The decreased irradiation time of 45 min results in significantly lowered amount of silver loading in the case of 1-Ag-45 min sample. On the other hand, increased irradiation time of 270 min does not provide the greatest Ag content among both series. In general, the Ag content is not predominantly defined by synthesis conditions, and is rather dependent on different factors.

Thus, a change in silver photoreduction mechanism on titania surface can be expected with variation of irradiation time and/or $AgNO_3$ concentration. To investigate these differences in the state of active component and related optical properties, diffuse reflectance spectroscopy was used.

Table 1 and Fig. 1 present the optical properties of the samples. The samples based on TiO_2 P25 demonstrate the presence of surface plasmon resonance (SPR) peak. The absorption edge of silver-containing systems is different from pristine TiO_2 indicating the presence of electronic interaction between Ag and the support [30].

The position of the SPR peaks mainly depends on the starting concentration of silver ions in the solution during the photoreduction procedure (see Table 1). At the same time, increased irradiation time did not lead to notable red shifts in the SPR peak wavelength, except for the 1-Ag-45 min sample, which supposedly had fewer opportunities for cluster aggregation. However, the intensity of optical absorption grows with the increase of both Ag^+ concentration and irradiation time that indicates the appearance of nanosized silver clusters on the surface of TiO_2 P25 in both cases. Interestingly, the greatest light absorption is observed for 1-Ag-270 min sample, while the largest SPR peak wavelength belongs to the sample with increased initial C_{Ag+} in the solution: 2-Ag-90 min. This hints at different growth mechanisms of silver clusters in the studied series. Notable widening of the SPR peaks with the increase of silver content in the initial solution can be explained by longitudinal character of plasmon resonance, further pointing out at the changes in particle shape [31]. Another possible reason of such peak behavior is the appearance of Ag_2O coating on the photodeposited Ag particles, which is formed during synthesis and causes a red-shift when more oxygen is adsorbed on the Ag cluster surface [32].

The optical bandgap values for the prepared samples are also listed in Table 1. The bandgap width for the initial TiO_2 P25 sample was calculated to be 3.10 eV that agrees well with published results for Degussa P25 in Ref. [33]. While no clear correlation between the bandgap width and preparation conditions is observed, the narrowing of the bandgap might be related to differences in Ag particle size. It is implied that electron transition type is not changed upon the addition of silver onto the surface of TiO_2 P25. Graphical representation of the Tauc plot method for each sample is shown in Fig. S1.

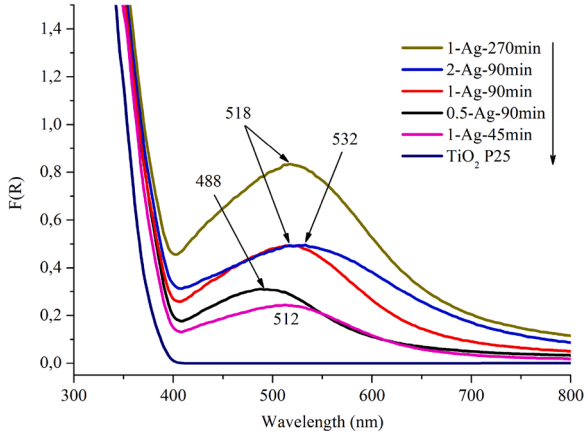

Fig. 1. Optical properties of the studied samples.

The obtained Ag-TiO_2 samples were studied with HR TEM, STEM-HAADF analysis, and EDS mapping technique. Fig. 2, a demonstrates the internal structure of the TiO_2 P25 support. The interplanar spacing corresponds to that of anatase, with a common particle size being 10−20 nm. The particles feature well-crystallized structure. The Ag photoreduction for 90 min from silver nitrate solution with concentration of 2.32 mM led to the distribution Ag NPs as small nanoparticles with predominant sizes of 1−2 nm (Fig.2, b, c). The formation of a small amount of Ag NPs with sizes of ~20 nm was observed.

According to the obtained data, 1-Ag-270 min sample possesses large Ag clusters with the sizes of 20−30 nm surrounded by a cloud of smaller 3−4 nm particles (Fig. S2, a). In addition, EDS mapping method shows that small Ag clusters are scattered throughout the sample surface (Fig. S2, b). The 1-Ag-90 min sample follows a similar pattern in STEM-HAADF demonstrating the lower amount of larger 30 nm particles (Fig. S2, c) in comparison with 1-Ag-270 min sample and smaller nanoparticles of ~1−2 nm (Fig. S2, d). HR TEM data confirms the presence of small silver nanoparticles through the surface of the sample (Fig. 2, c, d).

Fig. S2, f shows the results of STEM-HAADF analysis for 1-Ag-45 min sample. Similar to all samples studied above and prepared with C_{Ag+} = 2.32 mM, this photocatalyst possesses large Ag particles surrounded by a cloud of smaller 1−5 nm particles. However, in this case a decreased irradiation time coincides with downsized particles (about 20 nm) and leaves some areas completely free of such large particles. It points out at different growth character of small and large silver aggregates, with larger particles being formed in the solution and then descending on the catalyst surface after the process of homogeneous aggregation [34,35]. This may also explain the lack of SPR peak shift with nonetheless increasing light absorption in these sample series.

Additionally, the same analysis procedure was carried out with 2-Ag-90 min sample prepared with increased concentration of silver ions in the solution (see Fig. S2, g and h for STEM-HAADF and EDS images, respectively). Comparably to the previously discussed samples, 2-Ag-90 min features larger and smaller particles arranged in a similar fashion. However, the increased concentration of silver precursor leads to the formation of larger aggregates up to 50 nm in size, with smaller particles being present in lesser amount than in other studied samples. Although the size of the latter is 7−10 nm that is larger than in the other samples, their distribution is less uniform. This can be explained by the formation of larger particles in the solution medium rather than on the catalyst surface.

Fig. 3 presents the XRD results. It is shown that the position and intensity of anatase (PDF-2 #21-2172) and rutile (PDF-2 #21-1276) peaks do not change upon the addition of silver even with the increased initial concentration of silver (2-Ag-90 min sample). However, an additional peak at $2\theta = 32.2$ appears for all of the silver-containing samples corresponding to the phase of cubic Ag_2O (PDF-2 #41-1104). This may lead to a significant difference in photocatalytic activity during UV + Vis and visible irradiation experiments for the samples due to the possible formation of z-scheme Ag/Ag_2O/TiO_2 composites [2,3].

To investigate the influence of silver on TiO_2 electronic structure, Raman spectroscopy was used for the samples 0.5-Ag-90 min, 1-Ag-90 min, and 2-Ag-90 min. All four native TiO_2 Degussa P25 bands are present in all samples (see Fig. S3 for details) [36]. According to the results presented in Fig. 4, the addition of silver leads to a Raman shift from 142.4 cm^{-1} to 145.4 cm^{-1} for the characteristic peak of anatase nanoparticles indicating the presence of Ti^{3+} defects [37,38]. Observing similar shift in samples with different silver content, it can be suggested that only a fraction of loaded silver directly interacts with the titania surface.

Fig. 5 presents the zeta potential measurements of unmodified TiO_2 and the sample 1-Ag-270 min possessing the greatest light absorption. The isoelectric point of TiO_2 P25 is approximately 6.05, which is consistent with other studies (6.0 [39], 5.7 [40]). At the same time, the surface of Ag-containing photocatalyst 1-Ag-270 min is charged

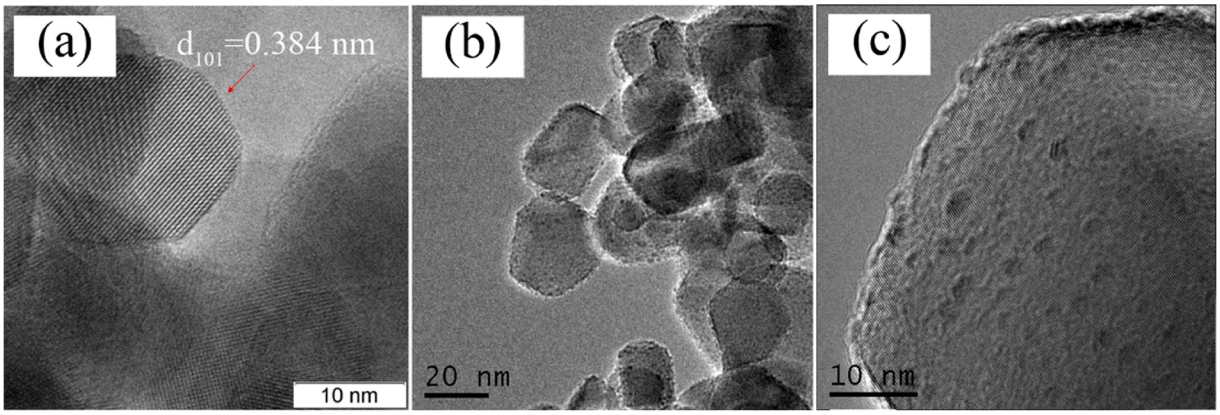

Fig. 2. Internal structure of prepared samples: (a) HR TEM of TiO_2 P25; (b, c) HR TEM of 1-Ag-90 min.

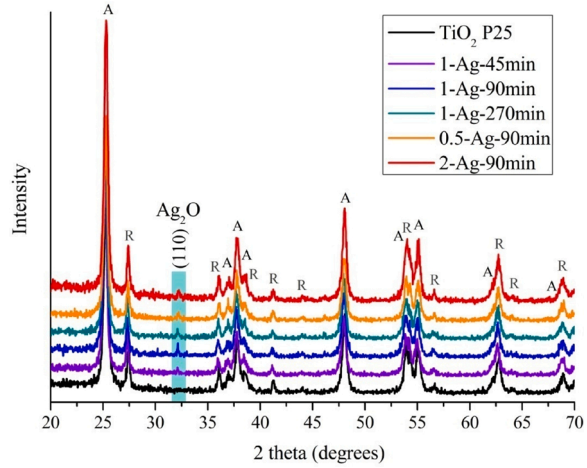

Fig. 3. Phase composition of studied samples. Symbols A and R stand for anatase and rutile phases, respectively.

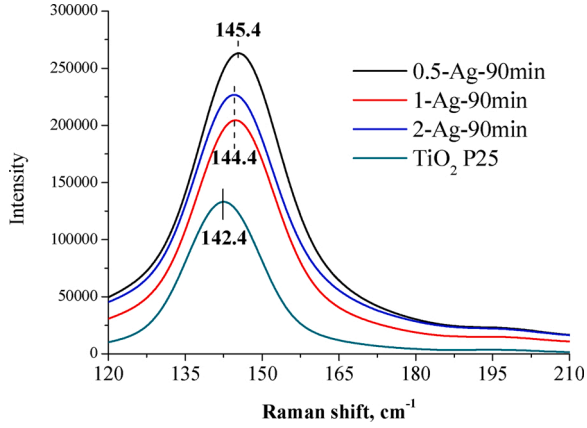

Fig. 4. Raman shift of anatase peak for samples 0.5-Ag-90 min, 1-Ag-90 min, 2-Ag-90 min and pristine TiO_2.

negatively with a different isoelectric point of 3.59 also corresponding to literature data [41]. It seems that the dye molecules in these cases tend to be adsorbed via different functional groups [42] providing differences in photodegradation mechanisms.

Table 2 and Fig. 6 show the results of photocatalytic studies. To provide better insight, optical properties from Table 1 are also presented. K_{uv+vis} and K_{vis} columns are intended for rate constants in

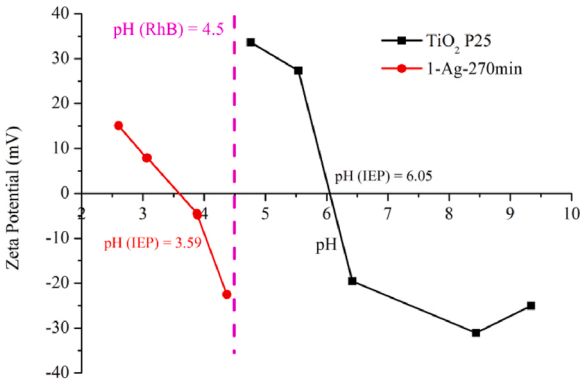

Fig. 5. Zeta potential measurements of TiO_2 P25 and 1-Ag-270 min samples.

Table 2
Photocatalytic activity of the samples.

Sample	λ_{SPR}, nm	E_g, eV	$K_{uv+vis}*10^3$, s^{-1}	$K_{vis}*10^3$, s^{-1}
1-Ag-45 min	512	2.80 ± 0.02	3.89	4.22
1-Ag-270 min	518	2.75 ± 0.02	**14.03**	3.15
0.5-Ag-90 min	488	2.91 ± 0.02	7.93	2.62
1-Ag-90 min	518	2.88 ± 0.02	**12.64**	3.44
2-Ag-90 min	532	2.83 ± 0.02	8.20	**4.61**
TiO_2 P25	–	3.10 ± 0.02	6.79	2.90

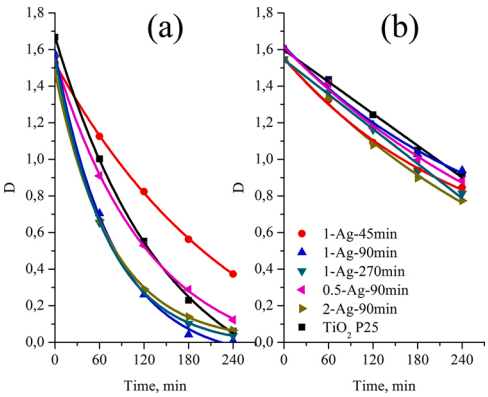

Fig. 6. Photocatalytic activity of all studied samples in UV + Vis (a) and Visible irradiation (b).

photocatalytic experiments using full spectrum of the lamp and visible light only, respectively.

It can be observed that the two featured irradiation modes lead to different catalysts being the most active amongst the whole series, which is presumably connected with the surface state and Ag-affected electronic properties of the studied samples. For UV + Vis mode, 1-Ag-90 min and 1-Ag-270 min are the most active samples, with their rate constant doubling that of unmodified support. At the same time, 1-Ag-45 min is even less active than pristine TiO_2. Coincidentally, this sample has an increased size of Ag clusters (Fig. S2, f) formed via photocatalytic reduction of Ag^+ on the surface of TiO_2 accompanied by the shortened time of irradiation and decreased number/size of silver clusters formed in the solution as a consequence of the latter. This hints further at the influence of Ag cluster size and origin on the catalyst behavior.

In the case of visible irradiation, the biggest rate constant is achieved by the 2-Ag-90 min sample having the largest "guest" Ag cluster size due to increased Ag^+ concentration in the initial solution. It goes along with the widest SPR peak located at 532 nm, which is the most red-shifted peak in the series indicating its contribution to the ability to absorb visible irradiation. Pristine TiO_2 P25 is active in visible light for the sole reason of RhB sensitization. The fact of 2-Ag-90 min and 1-Ag-45 min demonstrating the highest rate constant in visible irradiation, though under full spectrum of Xe lamp they did not show a comparable performance, may indicate the formation of $Ag/Ag_2O/TiO_2$ composites. In this case, absorption of UV photons by Ag_2O leads to a less involvement of TiO_2 and, as consequence, a decrease of photogenerated charge carriers, simultaneously the Ag^+ reduction reaction occurs on the surface of the photocatalysts with the help of remaining TiO_2-generated electrons [28].

Optical density curves during Rhodamine B decolorization experiment are presented in Fig. 7 for pristine TiO_2 P25 along with the most notable photocatalysts of this study. It can be seen that different sets of properties possessed by the samples provide a significant impact on the photocatalytic oxidation mechanism. Although the 1-Ag-90 min sample is the most active in UV + Vis decolorization, i.e. destruction of Rhodamine B dye molecule with a characteristic peak at 555 nm, it can be seen that intermediate products remain during the last hour of the experiment, which can be noted by higher absorption in the area of 200−300 nm compared to the experiment with unmodified titania. The change in RhB behavior in the presence of silver-containing catalyst is also noticeable after the first 60 min where the optical density curve intersects with the initial RhB absorption curve at the start of the experiment. In visible light, the same photocatalyst demonstrates a more selective dealkylation behavior [43] in comparison with all other samples, with characteristic peak at 260 nm responsible for conjugated structures featuring a notable blue shift with a lesser decrease in intensity. At the same time, 1-Ag-270 min sample behaves in a similar way to unmodified titania during both irradiation modes, showing a trend for general photodegradation of the substrate. Finally, 2-Ag-90 min sample demonstrates features of both processes, being notably less active in decolorization under UV + Vis illumination.

To investigate the influence of different radical species on the reaction of RhB decolorization, isopropyl alcohol (IPA) and benzoquinone (BQ) were used for trapping hydroxyl radicals and superoxide anions, respectively. Like in all previous catalytic experiments, change of optical density of the main RhB structure peak at 555 nm was chosen as analytic signal.

Fig. S4 shows the influence of IPA concentration (0.002–6 M) on the photocatalytic activity of pristine TiO_2 P25. According to the obtained data, C = 0.02 M and C = 0.2 M provide identical results indicating successfully trapped hydroxyl radicals. At the same time, excess C = 6 M completely prevents the reaction.

Fig. 8 shows comparison between pristine TiO_2 (a) and 1-Ag-90 min sample (b). It can be seen that in full spectrum of the lamp the addition of silver on TiO_2 surface certainly leads to an increase in overall decolorization activity of Ag-TiO_2 and provides increased concentration of both $^{\bullet}OH$ and $^{\bullet}O_2^-$.

In visible light, however, hydroxyl radicals are completely absent

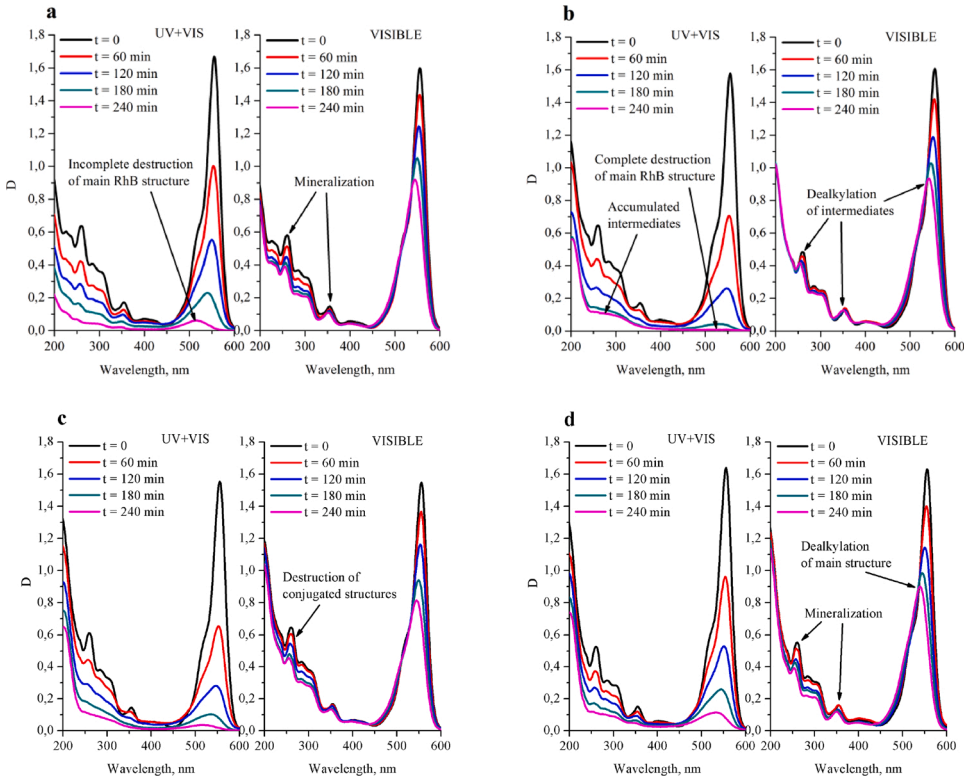

Fig. 7. Comparison of RhB optical density spectra during photocatalysis in UV + Vis and Visible irradiation for: (a) TiO_2 P25; (b) 1-Ag-90 min; (c) 1-Ag-270 min; (d) 2-Ag-90 min.

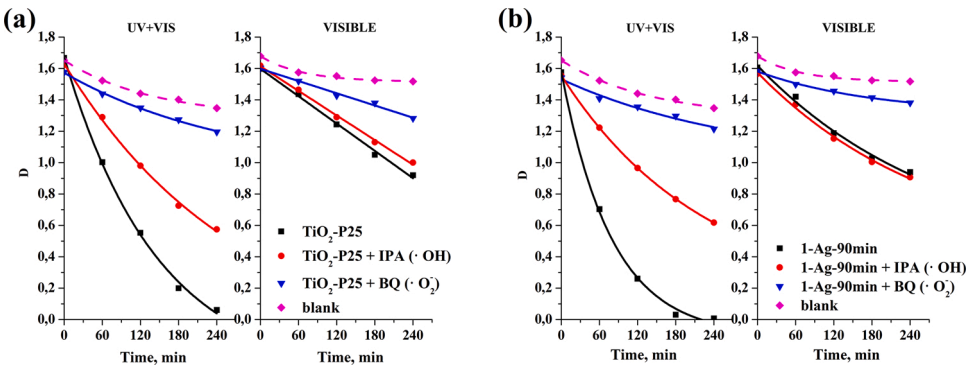

Fig. 8. Comparison of photocatalytic activity and mechanism details in UV + Vis and Visible irradiation for a) pristine TiO_2 and b) prepared 1-Ag-90 min sample.

when 1-Ag-90 min is employed. The observed facts allow concluding that the increase in ·OH concentration during UV + Vis irradiation is attributed to better charge separation provided by silver nanoparticles on the titania surface, and not to the ability of silver itself to facilitate ·OH generation on its surface in spite of shifted absorption edge and more narrow bandgap. Moreover, whereas TiO_2 P25 is confirmed to generate hydroxyl radicals of its own during visible light irradiation [44], the presence of silver negates the phenomenon leading to a more selective dealkylation behavior of silver-containing samples observed in this study.

4. Conclusions

To summarize the obtained results, both the irradiation time and initial silver concentration in the solution influence on the formation of silver clusters and the resulting optical properties. It has been shown that the formation of silver clusters occurs both photochemically and photocatalytically, with large clusters appearing in the solution medium as a result of irradiation and descending to the titania surface, depending in size on initial Ag^+ concentration mostly. The smaller silver clusters appear directly on the surface via photocatalytic reduction of silver ions and their growth is inhibited by the presence of larger clusters coming from the solution. With an increase in Ag^+ concentration, the photocatalytic formation of photoreduced surface clusters is inhibited further as it is shown for 2-Ag-90 min sample. At the same time, prolonged irradiation leads to the photocatalytical growth of silver clusters in 1-Ag-270 min sample. This suggests that the number of active sites on the TiO_2 surface is the limiting factor of photocatalytical growth for silver particles. Moreover, when Ag^+ concentration is further increased in the solution, silver photoreduction process tends to occur rather in close proximity to the surface than on the surface itself leading to the formation of larger particles weakly bonded with the sample surface in this particular case.

Such growth mechanisms diversely affect optical properties of the samples: while irradiation time is generally responsible for absorption intensity, initial Ag^+ concentration is mainly responsible for the SPR peak position. One of the notable examples is the 2-Ag-90 min sample demonstrating a red shift indicating the presence of larger particles and wider size distribution in comparison with the 1-Ag-90 min which is otherwise close to it in terms of optical properties.

The behavior of the samples in visible and UV + Vis irradiation experiments also differs significantly with the change in Ag cluster size and bandgap width. It has been observed that despite the highest RhB decolorization activity in full spectrum of the lamp, the sample 1-Ag-90 min is the most selective towards dealkylation of the main structure of the substrate instead of complete mineralization during visible irradiation. This behavior has been associated with the smallest Ag cluster size and widest distribution of these clusters as confirmed by STEM-HAADF, EDS and HRTEM methods. At the same time, 2-Ag-90 min sample possessing the largest Ag clusters behaves in a similar fashion to pristine TiO_2 in visible light providing a less selective destruction of RhB structure and featuring the highest rate constant in the whole study, with SPR position shifted to 532 nm in comparison with 518 nm of 1-Ag-90 min sample. This indicates better involvement of electrons during the visible light irradiation for 2-Ag-90 min. It has been also demonstrated that the presence of silver negates the formation of hydroxyl radicals in visible light promoting the formation of superoxide anions at the same time, which describes the behavior of 1-Ag-90 min sample further.

The sample 1-Ag-45 min clearly underperforms in the full spectrum of the lamp showing similar behavior to 2-Ag-90 min due to the presence of partially reduced silver that leads to a decrease in photoactivity. The rate constant for this sample is lower than for pristine TiO_2 indicating that electrons are utilized preferably in the subsequent Ag^+ reduction than in generation of superoxide anions on the surface of the on-top Ag° clusters. In visible light, however, surface Ag cations are not reduced because the electrons come exclusively from the process of Rhodamine B photosensitization and accumulate behind the Schottky barrier, thus notably increasing the photocatalytic performance of the sample.

Such differences in photocatalytic activity result from silver deposited on the TiO_2 surface in a different manner during the same photoreduction process. With that, when the Ag^+ exists in excess with respect to the O^- active sites or there is not enough time for a more complete photoreduction, silver oxide is deposited on TiO_2 with metallic silver growing on top of the resulting particles. These systems change their composition during the UV irradiation, with TiO_2-generated electrons participating in Ag^+ photoreduction on the site. However, such catalysts are better at utilizing photosensitized electrons under visible light and are able to facilitate photodegradation of organic substances without using higher energy irradiation.

When synthesis conditions favor a more complete photoreduction of deposited silver during the preparation stage, another kind of heterojunction is being formed, with Ag_2O capping the surface of the metallic silver cluster and forming a core-shell particle with Z-scheme electron transfer. Such systems are more effective in full spectrum of the lamp ($\lambda > 300$ nm) being able to accumulate surface-generated electrons and provide better separation of charge carriers. However, when UV part of the spectrum is absent, such catalysts lose the ability to produce hydroxyl radicals, even more than pristine TiO_2 facilitating mild oxidation of organic substances with an increased number of superoxide anions.

CRediT authorship contribution statement

A.A. Vodyankin: Investigation, Data curation, Writing - original draft. **Yu.A. Belik:** Investigation, Visualization, Formal analysis. **V.I. Zaikovskii:** Methodology, Software. **O.V. Vodyankina:** Conceptualization, Methodology, Supervision.

Declaration of Competing Interest

The authors declare that they have no known competing financial

interests or personal relationships that could have appeared to influence the work reported in this paper.

Acknowledgement

This work was supported by Russian Science Foundation (project number 19-73-30026).

Appendix A. Supplementary data

Supplementary material related to this article can be found, in the online version, at doi:https://doi.org/10.1016/j.jphotochem.2020.113091.

References

[1] V. Torbina, A. Vodyankin, S. Ten, G. Mamontov, M. Salaev, V. Sobolev, O. Vodyankina, Ag-Based Catalysts in Heterogeneous Selective Oxidation of Alcohols: A Review, Catalysts 8 (2018) 447, https://doi.org/10.3390/catal8100447.

[2] H.-T. Ren, J. Han, T.-T. Li, Y. Liang, M.-Z. Jing, S.-M. Jiang, J.-H. Lin, C.-W. Lou, Facile preparation of PAN@Ag–Ag_2O/TiO_2 nanofibers with enhanced photocatalytic activity and reusability toward oxidation of As(III), J. Mater. Sci. 55 (2020) 11310–11324, https://doi.org/10.1007/s10853-020-04835-9.

[3] H.-L. Yua, Q.-X. Wu, J. Wang, L.-Q. Liu, B. Zheng, C. Zhang, Y.-G. Shen, C.-L. Huang, B. Zhou, J.-R. Jia, Simple fabrication of the Ag-Ag_2O-TiO_2 photocatalyst thin films on polyester fabrics by magnetron sputtering and its photocatalytic activity, App. Surf. Sci. 503 (2020), 144075,, https://doi.org/10.1016/j.apsusc.2019.144075.

[4] S. Akel, R. Dillert, N.O. Balayeva, R. Boughaled, J. Koch, M. El Azzouzi, D. W. Bahnemann, Ag/Ag_2O as a Co-catalyst in TiO_2 photocatalysis: effect of the Co-Catalyst/Photocatalyst mass ratio, Catalysts 8 (2018) 647, https://doi.org/10.3390/catal8120647.

[5] C. Liu, C. Cao, X. Luo, S. Luo, Ag-bridged Ag_2O nanowire network/TiO_2 nanotube array p–n heterojunction as a highly efficient and stable visible light photocatalyst, J. Hazard. Mater. 285 (2015) 319–324, https://doi.org/10.1016/j.jhazmat.2014.12.020.

[6] H.-T. Ren, Q. Yang, Fabrication of Ag_2O/TiO_2 with enhanced photocatalytic performances for dye pollutants degradation by a pH-induced method, App. Surf. Sci 396 (2017) 530–538, https://doi.org/10.1016/j.apsusc.2016.10.191.

[7] M. Coto, G. Divitini, A. Dey, S. Krishnamurthy, N. Ullah, C. Ducati, R. Vasant Kumar, Tuning the properties of a black TiO_2-Ag visible light photocatalyst produced by rapid one-pot chemical reduction, Mater. Today Chem. 4 (2017) 142–149, https://doi.org/10.1016/j.mtchem.2017.03.002.

[8] S. Khan, I.A. Qazi, I. Hashmi, M. Ali Awan, N. Sadaf Zaidi, Synthesis of silver-doped titanium TiO_2 powder-coated surfaces and its ability to inactivate Pseudomonas aeruginosa and Bacillus subtilis, J. Nanomater. (2013), 531010,, https://doi.org/10.1155/2013/531010.

[9] M.J. Kim, G.-H. Han, S.H. Lee, H.W. Jung, J.W. Choung, C.H. Kim, K.-Y. Lee, CeO_2 promoted Ag/TiO_2 catalyst for soot oxidation with improved active oxygen generation and delivery abilities, J. Hazard. Mater. 384 (2020), 121341,, https://doi.org/10.1016/j.jhazmat.2019.121341.

[10] S.F. Chin, S.C. Pang, F.E.I. Dom, Sol-gel synthesis of silver/titanium dioxide (Ag/TiO_2) core-shell nanowires for photocatalytic applications, Mater. Lett. 65 (2011) 2673–2675, https://doi.org/10.1016/j.matlet.2011.05.076.

[11] H.-C. Tseng, Y.-W. Chen, Facile synthesis of Ag/TiO_2 by photoreduction method and its degradation activity of methylene blue under UV and visible light irradiation, Mod. Res. Catal. 9 (2020) 97149, https://doi.org/10.4236/mrc.2020.91001.

[12] K. Kawahara, K. Suzuki, Y. Ohko, T. Tatsuma, Electron transport in silver-semiconductor nanocomposite films exhibiting multicolor photochromism, Phys. Chem. Chem. Phys. 7 (2005) 3851–3855, https://doi.org/10.1039/B511489F.

[13] K. Wenderich, G. Mul, Methods, mechanism, and applications of Photodeposition in photocatalysis: a review, Chem. Rev. 116 (2016) 14587–14619, https://doi.org/10.1021/acs.chemrev.6b00327.

[14] H. Liang, Z. Jia, H. Zhang, X. Wang, J. Wang, Photocatalysis oxidation activity regulation of Ag/TiO_2 composites evaluated by the selective oxidation of Rhodamine B, Appl. Surf. Sci. 422 (2017) 1–10, https://doi.org/10.1016/j.apsusc.2017.05.211.

[15] S. Wang, Z. Han, T. Di, R. Li, S. Liu, Z. Cheng, Preparation of pod-shaped TiO_2 and Ag@TiO_2 nano burst tubes and their photocatalytic activity, R. Soc. Open Sci. 6 (2019), 191019,, https://doi.org/10.1098/rsos.191019.

[16] Y. Gao, W. Zhang, P. Liu, Enhanced photocatalytic efficiency of TiO_2 membrane decorated with Ag and Au nanoparticles, Appl. Sci. 8 (2018) 945, https://doi.org/10.3390/app8060945.

[17] P.V. Viet, B.T. Phan, D. Mott, S. Maenosono, T.T. Sang, C.M. Thi, L.V. Hieu, Silver nanoparticle loaded TiO_2 nanotubes with high photocatalytic and antibacterial activity synthesized by photoreduction method, J. Photochem. Photobiol. A 352 (2018) 106–112, https://doi.org/10.1016/j.jphotochem.2017.10.051.

[18] Ch. Girginov, P. Stefchev, P. Vitanov, Hr Dikov, Silver doped TiO_2 photocatalyst for methyl orange degradation, J. Eng. Sci. Tech. Rev. 5 (2012) 14–17, https://doi.org/10.25103/jestr.054.03.

[19] A. Valentine Rupa, D. Manikandan, D. Divakar, T. Sivakumar, Effect of deposition of Ag on TiO_2 nanoparticles on the photodegradation of Reactive Yellow-17, J. Hazard. Mater. 147 (2007) 906–913, https://doi.org/10.1016/j.jhazmat.2007.01.107.

[20] N. Sobana, M. Muruganadham, M. Swaminathan, Nano-Ag particles doped TiO_2 for efficient photodegradation of Direct azo dyes, J. Mol. Catal. A Chem. 258 (2006) 124–132, https://doi.org/10.1016/j.molcata.2006.05.013.

[21] M. Hari, S.A. Joseph, S. Mathew, P. Radhakrishnan, V.P.N. Nampoori, Band-gap tuning and nonlinear optical characterization of Ag:TiO_2 nanocomposites, J. Appl. Phys. 112 (2012), 074307,, https://doi.org/10.1063/1.4757025.

[22] Y. Zhang, S. Zhou, X. Su, J. Xu, G. Nie, Y. Zhang, Y. He, S. Yu, Synthesis and characterization of Ag-loaded p-type TiO_2 for adsorption and photocatalytic degradation of tetrabromobisphenol A, Water Environ. Res. (2019) 1–10, https://doi.org/10.1002/wer.1264.

[23] Q. Zeng, X. Xie, X. Wang, Y. Wang, G. Lu, D.Y.H. Pui, J. Sun, Enhanced photocatalytic performance of Ag@TiO_2 for the gaseous acetaldehyde photodegradation under fluorescent lamp, Chem. Eng. J. 341 (2018) 83–92, https://doi.org/10.1016/j.cej.2018.02.015.

[24] I. Tunc, M. Bruns, H. Gliemann, M. Grunzea, P. Koelsch, Bandgap determination and charge separation in Ag@TiO_2 core shell nanoparticle films, Surf. Interface Anal. 42 (2010) 835–841, https://doi.org/10.1002/sia.3558.

[25] M.Q. Tran, Y. Yamaguchi, K. Yamatoya, S. Horikoshi, K. Nakata, Rewritable superhemophobic and superhemophilic wettability pattern based on titanium dioxide with Ag loading, Inorg. Chem. Commun. 96 (2018) 1–4, https://doi.org/10.1016/j.inoche.2018.07.043.

[26] S.X. Liu, Z.P. Qu, X.W. Han, C.L. Sun, A mechanism for enhanced photocatalytic activity of silver-loaded titanium dioxide, Catal. Today 93–95 (2004) 877–884, https://doi.org/10.1016/j.cattod.2004.06.097.

[27] J. Diaz-Angulo, I. Gomez-Bonilla, C. Jimenez-Tohapanta, M. Mueses, M. Pinzona, F. Machuca-Martinez, Visible-light activation of TiO_2 by dye-sensitization for degradation of pharmaceutical compounds, Photochem. Photobiol. Sci. 18 (2019) 897–904, https://doi.org/10.1039/C8PP00270C.

[28] A.A. Evstratov, C. Chis, A.A. Malygin, J.-M. Taulemesse, P. Gaudon, T. Vincent, Free charge carrier repartition over the surface of photosensitive materials: why and how to manage? Russ. J. Gen. Chem. 78 (2008) 1070–1080, https://doi.org/10.1134/S107036320805040X.

[29] X. Liu, N. Chen, Y. Li, D. Deng, X. Xing, Y. Wang, A general nonaqueous sol-gel route to g-C_3N_4-coupling photocatalysts: the case of Z-scheme g-C_3N_4/TiO_2 with enhanced photodegradation toward RhB under visible-light, Sci. Rep. 6 (2016) 39531, https://doi.org/10.1038/srep39531.

[30] P. Peerakiatkhajorn, C. Chawengkijwanich, W. Onreabroy, S. Chiarakorn, Novel photocatalytic Ag/TiO_2 thin film on polyvinyl chloride for gaseous BTEX treatment, Mater. Sci. Forum. 712 (2012) 133–145, https://doi.org/10.4028/www.scientific.net/MSF.712.133.

[31] A.A. Ashkarran, A. Bayat, Surface plasmon resonance of metal nanostructures as a complementary technique for microscopic size measurement, Int. Nano Lett. 3 (2013) 1–10, https://doi.org/10.1186/2228-5326-3-50.

[32] D.S. Afanasev, V.F. Anufrienko, S.F. Ruzankin, T.V. Larina, N.I. Kuznetsova, V. I. Bukhtiyarov, Effect of oxygen adsorption on the surface plasmon resonance of oxide-supported silver nanoparticles, Dokl. Phys. Chem. 436 (2011) 23–25, https://doi.org/10.1134/S0012501611020035.

[33] J.F. Guayaquil-Sosa, B. Serrano-Rosales, P.J. Valadés-Pelayo, H. de Lasa, Photocatalytic hydrogen production using mesoporous TiO_2 doped with Pt, Appl. Catal. B: Envir. 211 (2017) 337–348, https://doi.org/10.1016/j.apcatb.2017.04.029.

[34] M. Szymańska-Chargot, A. Gruszecka, A. Smolira, K. Bederski, K. Głuch, J. Cytawa, L. Michalak, Formation of nanoparticles and nanorods via UV irradiation of $AgNO_3$ solutions, J. Alloys. Compd. 486 (2009) 66–69, https://doi.org/10.1016/j.jallcom.2009.07.094.

[35] J. Taing, M.H. Cheng, J.C. Hemminger, Photodeposition of Ag or Pt onto TiO_2 nanoparticles decorated on step edges of HOPG, ACS Nano 5 (2011) 6325–6333, https://doi.org/10.1021/nn201396v.

[36] E.D. Fakhrutdinova, A.V. Shabalina, M.A. Gerasimova, A.L. Nemoykina, O. V. Vodyankina, V.A. Svetlichnyi, Highly defective dark nano titanium dioxide: preparation via pulsed laser ablation and application, Materials 13 (2020) 1–17, https://doi.org/10.3390/ma13092054.

[37] Y. Zhou, C. Chen, N. Wang, Y. Li, H. Ding, Stable Ti3+ self-doped anatase-rutile mixed TiO_2 with enhanced visible light utilization and durability, J. Phys. Chem. C. 120 (2016) 6116–6124, https://doi.org/10.1021/acs.jpcc.6b00655.

[38] L.M. Santos, W.A. Machado, M.D. França, K.A. Borges, R. Paniago, A.O. T. Patrocinio, A.E.H. Machado, Structural characterization of Ag-doped TiO_2 with enhanced photocatalytic activity, RSC Adv. 5 (2015) 103752–103759, https://doi.org/10.1039/C5RA22647C.

[39] K. Suttiponparnit, J. Jiang, M. Sahu, S. Suvachittanont, T. Charinpanitkul, P. Biswas, Role of surface area, primary particle size, and crystal phase on titanium dioxide nanoparticle dispersion properties, Nanoscale Res. Lett. 6 (2011) 27, https://doi.org/10.1007/s11671-010-9772-1.

[40] W.-B. Tsai, J.-Y. Kao, T.-M. Wu, W.-T. Cheng, Dispersion of titanium oxide nanoparticles in aqueous solution with anionic stabilizer via ultrasonic wave, J. Nanoparticles 11 (2016) 1–9, https://doi.org/10.1155/2016/6539581.

[41] M. Jose, P. Sienkiewicz, K. Szymańska, D. Darowna, D. Moszyński, Z. Lendzion-Bieluń, K. Szymański, S. Mozia, Influence of preparation procedure on

physicochemical and antibacterial properties of titanate nanotubes modified with silver, Nanomaterials 9 (2019) 795, https://doi.org/10.3390/nano9050795.
[42] F. Chen, J. Zhao, H. Hidaka, Highly selective deethylation of rhodamine B: adsorption and photooxidation pathways of the dye on the TiO_2/SiO_2 composite photocatalyst, Int. J. Photoenergy 5 (2003) 209–217, https://doi.org/10.1155/S1110662X03000345.
[43] Z.Y. Lin, J. Xiao, J.H. Yan, P. Liu, L.H. Li, G.W. Yang, Ag/AgCl plasmonic cubes with ultrahigh activity as advanced visible-light photocatalysts for photodegrading dyes, J. Mater. Chem. A 3 (2015) 7649–7658, https://doi.org/10.1039/C5TA00942A.
[44] A.M. Abdullah, M.Á. Gracia-Pinilla, S.C. Pillai, K. O'Shea, UV and visible light-driven production of hydroxyl radicals by reduced forms of N, F, and P codoped titanium dioxide, Molecules 24 (2019) 2147, https://doi.org/10.3390/molecules24112147.